Critical analysis of the relations between the velocities of elastic waves and effective anisotropy of ice polycrystals

A. Maurel[1], J.-F. Mercier[2], and M. Montagnat[3]

[1] Institut Langevin, CNRS, ESPCI ParisTech, 1 rue Jussieu, 75005 Paris, France
[2] Poems, CNRS, ENSTA ParisTech, INRIA, 828 boulevard des Maréchaux 91762 Palaiseau, France
[3] LGGE, CNRS, Université Grenoble Alpes, 38041 Grenoble, France.

Correspondence to: A. Maurel (agnes.maurel@espci.fr)

Abstract. Sonic logging measurements in ice core boreholes allow for the determination of the velocities of the elastic waves used as a proxy for the variation of ice polycrystal anisotropy due to the texture (or fabric) evolution with depth. This needs an inversion from the velocities deduced from the measured times of flight and the anisotropy of the ice polycrystal where the elastic waves

5 have propagated. A classical model used in glaciology is based on the so-called velocity, or slowness, average method. Namely the elastic velocities in a polycrystal are calculated considering the average of the velocities, or the average of the slownesses, along the ray path from the emitter to the receiver of the logger. There are several pitfalls in this approach and it is the scope of the present paper to illustrate them and to propose a consistent inversion procedure. This is done by deriving the phase

10 velocities in the effective medium obtained by averaging the elastic tensor.

1 Introduction

Wave propagation in glaciology most often is regarded in the context of seismic waves, *e.g.* (*Kohnen*, 1974; *Blankenship et al.*, 1987). More recently, the interest has been renewed with the idea of using in situ velocity measurement in boreholes as an alternative to usual thin section analysis. A first

15 campagne at Dome C has been performed using a classical sonic logger (*Gusmeroli et al.*, 2012). Sonic logging is based on the measure of the times of flight of elastic waves propagating over a short distance (typically few meters). This campagne has revealed the sensitivity of the elastic velocities on the degree of anisotropy of ice polycrystals with a cluster-type texture (*c*-axis orientation clustered around the vertical direction), that varies with depth. Nevertheless, the changes in the velocities

20 remain small, which motivates the development of accurate models needed to make the inversion from the elastic velocities to the local ice anisotropy.

In a previous paper (*Maurel et al.*, 2015), we applied a classical model for wave propagation in polycrystals to the particular textures as found in ice recovered from deep ice cores, namely clusters (with vertical transverse isotropy, VTI) and girdles with horizontal transverse isotropy, HTI. The

25 model relies on the wave equation being written using the effective elasticity tensor. This latter is the ensemble average of the elasticity tensors for all possible realizations of the crystallographic orientations of the grains within the polycrystal. Basically, let us start from the wave equation written for a particular realization

$$\rho\omega^2 u_a + \frac{\partial}{\partial x_b} c_{abcd} \frac{\partial}{\partial x_c} u_d = 0, \tag{1}$$

30 with c_{abcd} the elasticity tensor being space dependent (from grain to grain), and $u_{a,d}$ the component of the elastic displacement along the axis $\mathbf{e}_{a,d}$ (and a, d takes the values 1,2,3); also, in the above equation, repeated indices means summation (Einstein convention). The most representative realization corresponds to the wave equation in an homogeneous medium

$$\rho\omega^2 u_a + \langle c_{abcd} \rangle \frac{\partial^2}{\partial x_b \partial x_c} u_d \simeq 0, \tag{2}$$

35 where we have expand $c_{abcd} = \langle c_{abcd} \rangle + \delta c_{abcd}$, with $\langle c_{abcd} \rangle$ the ensemble average of c_{abcd}. Here δc_{abcd} is a measure of the changes in anisotropy from grain to grain, with typical relative amplitude $\epsilon = \delta c/c$ being assumed to be small. Because $\langle \delta c_{abcd} \rangle = 0$ by construction, the model is accurate up to ϵ^2.

Starting in the 1960s, these methods, often referred as stochastic methods, have being developed
40 (*Keller*, 1964; *Karal and Keller*, 1964) and preferred to the methods based on spatial averages. These latter are based on the intuitive argument that the time of flight of the wave through successive grains along the ray path is the correct "extensive" quantity to be considered. If one considers that the grains have roughly the same size, this is equivalent to average the inverse of the velocities, called slowness (and these methods are called "slowness average methods"). Although it is sometimes thought that
45 ergodicity ensures the two approaches to be equivalent, the slowness average methods have at least two disadvantages: first, they do not rely on a rigorous mathematical formalism, and secondly, there is no guaranty that the obtained velocities satisfy the expected anisotropy of the polycrystal at large scale.

This is the main subject of the present paper to illustrate the unphysical results that such slowness
50 average methods can give, and to quantify the resulting error for practical situations. To that aim, we consider the simplest case of cluster textures in ice. Clusters have vertical transverse isotropy, which means that the horizontal plane is isotropic. We show that the slowness average method predicts that a wave propagating along the vertical axis is associated to two different shear velocities, which is clearly unphysical since the polarizations of the shear waves belong to the plane of isotropy.

55 Although two shear velocities should be found, Bennett obtained a unique shear velocity using the slowness average method for clustered textures (*Bennett*, 1968), and this result is largely used in the community of glaciology, see *e.g. Vélez et al.* (2016). It is not possible to ignore Bennett's calculations and it is the subject of a second part in this paper: we show that Bennett uses an unjustified qualitative argument which leads to erroneous expressions of the shear velocities in single ice.

60 This error has nothing to do with the average method that he uses latter; the error really occurs at the starting point of his calculation.

When needed, the values of the elastic constants for ice single crystals are taken from *Bennett* (1968):

$$\text{Ice single crystal} \begin{cases} A = 14.06 \times 10^9 \ \text{N.m}^{-2}, \ C = 15.24 \times 10^9 \ \text{N.m}^{-2}, \ L = 3.06 \times 10^9 \ \text{N.m}^{-2}, \\ N = 3.455 \times 10^9 \ \text{N.m}^{-2}, \ F = 5.88 \times 10^9 \ \text{N.m}^{-2}, \ \rho = 917 \ \text{kg/m}^3. \end{cases} \tag{3}$$

65 2 Classical results on polycrystal effective anisotropy and wave propagation in anisotropic media

In this section, we just recall classical results on the elasticity tensor of polycrystals, regarded at the scale of many grains as an equivalent "single" crystal, and on the propagation of elastic waves in single crystal. This allows to introduce the notations that will be used in the sequel, and to clarify in
70 a self consistent way some properties that will be needed.

2.1 Characteristics of the polycrystal resulting from anisotropy from grain to grain

We consider that each grain within the polycrystal is composed of the same single crystal with hexagonal symmetry being characterized by its elasticity tensor c^0_{ijkl}, written as C^0 in the Voigt's notation

$$75 \quad \mathsf{C}^0 = \begin{pmatrix} A & A-2N & F & 0 & 0 & 0 \\ A-2N & A & F & 0 & 0 & 0 \\ F & F & C & 0 & 0 & 0 \\ 0 & 0 & 0 & L & 0 & 0 \\ 0 & 0 & 0 & 0 & L & 0 \\ 0 & 0 & 0 & 0 & 0 & N \end{pmatrix}. \tag{4}$$

This corresponds to an elasticity tensor c^0_{ijkl} being expressed in the frame of its principal axes, with the c-axis being oriented along $\mathbf{e}_3$, hereafter referred as the vertical axis. We use the elasticity tensor in Voigt's notation (*Voigt*, 1928), C_{IJ} with the standard correspondences

$$\begin{cases} c_{ijk\ell} \to C_{IJ}, \\ \text{for} \quad (i,j) \to I, \quad (k,l) \to J, \\ \text{and} \quad (1,1) \to 1, (2,2) \to 2, (3,3) \to 3, \\ \quad\quad (3,2), (2,3) \to 4, (3,1), (1,3) \to 5, (1,2), (2,1) \to 6. \end{cases} \tag{5}$$

80 Next, for an arbitrary direction of the c-axis (Fig. 1), namely

$$\hat{\mathbf{c}} = (\sin\theta\cos\varphi, \sin\theta\sin\varphi, \cos\theta), \tag{6}$$

the elasticity tensor c_{ijkl} is deduced from c_{ijkl}^0 following

$$c_{abcd} = \mathsf{R}_{ia}\mathsf{R}_{jb}\mathsf{R}_{kc}\mathsf{R}_{ld}c_{ijk\ell}^0, \tag{7}$$

with R the rotation matrix

85
$$\mathsf{R} \equiv \begin{pmatrix} \cos\theta\cos\varphi & \cos\theta\sin\varphi & -\sin\theta \\ -\sin\varphi & \cos\varphi & 0 \\ \sin\theta\cos\varphi & \sin\theta\sin\varphi & \cos\theta \end{pmatrix}, \tag{8}$$

and obviously, c_{abcd} depends on (θ, φ) which are the usual angles in spherical coordinates.
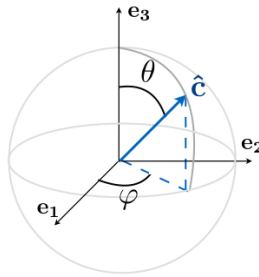
Figure 1. Usual spherical angles (φ, θ) used for the orientation of the c-axis, ($\hat{\mathbf{c}}$ is an unitary vector).

The anisotropy at the macroscopic scale (at the scale of many grains) result from the many (or few) possible orientations of the c-axis in each grain. This distribution of c-axis is defined by a probability distribution function $p(\theta, \varphi)$, and $p(\theta, \varphi)$ has to satisfy

90
$$\int \mathrm{d}\Omega\, p(\theta, \varphi) = 1, \quad \text{with } \mathrm{d}\Omega = \sin\theta\, \mathrm{d}\theta\mathrm{d}\varphi. \tag{9}$$

When needed, the elasticity tensor c_{ijkl}^{eff} of the polycrystal can be calculated by means of the average of the elasticity tensors of the grains following

$$c_{ijkl}^{\mathrm{eff}} = \int \mathrm{d}\Omega\; p(\varphi, \theta)c_{ijkl}, \quad C_{IJ}^{\mathrm{eff}} = \int \mathrm{d}\Omega\; p(\varphi, \theta)C_{IJ}, \tag{10}$$

with the same index convention, Eq. (5), between the elasticity tensor c_{ijkl}^{eff} and the Voigt matrix
95 C_{IJ}^{eff}.

2.2 Wave propagation – The Christoffel equation

The propagation of monochromatic waves of frequency ω in single crystals is described by the wave equation

$$\rho\omega^2 u_a + c_{abcd}\frac{\partial^2}{\partial x_b \partial x_c}u_d = 0. \tag{11}$$

100 with the same notations as in Eq. (1). Denoting $\mathbf{k} = k(n_1, n_2, n_3)$ the wavevector (k is the wavenumber), the elastic displacement reads $u_a = U_a e^{ik(n_1 x_1 + n_2 x_2 + n_3 x_3)}$ leading to $\rho\omega^2 U_a - k^2 c_{abcd} n_b n_c U_d = 0$. This system of equations admits non zero solution for (U_1, U_2, U_3) if the discriminant of the matrix $\rho\omega^2 \delta_{ad} - k^2 c_{abcd} n_b n_c$ vanishes, leading to a dispersion relation $D(\omega, k) = 0$. One gets the dispersion relation in the classical form of the Christoffel equation introducing the phase velocity $V = \omega/k$,

105 thus

$$\text{Det}\left[\rho V^2 \delta_{ad} - c_{abcd} n_b n_c\right] = 0. \tag{12}$$

The Christoffel equation admits in general three solutions $V = V_P, V_{SH}, V_{SV}$ which correspond to one longitudinal wave and two transverse waves.

It is important to stress at this point that the three values of V^2 being the eigenvalues of the matrix

110 $c_{abcd} n_b n_c / \rho$, they do not depend on the particular frame $(\mathbf{e}_1, \mathbf{e}_2, \mathbf{e}_3)$ used to express c_{abcd}. To the contrary, the eigenvectors (U_1, U_2, U_3) associated to the eigenvalues obviously depend on the frame where they are expressed.

3   On the non pertinence of averaging the acoustical slowness or the velocities

In this section, we compare the elastic velocities obtained from the slowness average method, as

115 used in *Bennett* (1968); *Gusmeroli et al.* (2012); *Vélez et al.* (2016), and the elastic velocities obtained from the effective medium theory (*Maurel et al.*, 2015). Omitting the distinction between slowness/velocity and compliance/elasticity tensors, which remains incidental at this stage, the two approaches are as follow

---

Velocities from the velocity averaging method

First, solve the Christoffel equation for given (θ, φ) :
$$V(\theta, \varphi) = V_P, V_{SV}, V_{SH} \text{ are the roots of } \text{Det}\left[\rho V^2 \delta_{il} - c_{ijkl} n_j n_k\right],$$

Then compute the average of the slowness, from which: $V^{\text{av}} = \left[\int \mathrm{d}\Omega\, p(\theta, \varphi) V^{-1}(\theta, \varphi)\right]^{-1}$

---

(13)

120 and we will see that this may lead to inconsistent results. Alternatively,

---

Velocities of the effective medium

First, compute the effective elasticity tensor: $c_{ijkl}^{\text{eff}} = \int \mathrm{d}\Omega\, p(\theta, \varphi) c_{ijkl}$,

Then, solve the Christoffel equation:
$$V = V_P^{\text{eff}}, V_{SV}^{\text{eff}}, V_{SH}^{\text{eff}} \text{ are the roots of } \text{Det}\left[\rho V^2 \delta_{il} - c_{ijkl}^{\text{eff}} n_j n_k\right],$$

$$(14)$$

and we will see that this leads to consistent results.

Below, we report examples of textures with Vertical Transverse Isotropy (VTI), see *e.g.* Fig. 3, for which velocity or slowness averaging methods lead to inconsistent results. Vertical transverse isotropy means that the horizontal plane (transverse to the vertical direction) is a plane of isotropy. This is true for any mechanical response of a polycrystal sample (at least in the elastic regime) and this has to be true for the response of the polycrystal to an incident wave. This is because a wave produces nothing else than a time periodic elastic stress. Now, if one considers the propagation of a wave along the vertical direction $\mathbf{e}_3$, the shear displacements are in-plane displacements in the plane $(\mathbf{e}_1, \mathbf{e}_2)$, that is in the plane where the response of the polycrystal is isotropic. Thus, there is a unique shear velocity in this particular case ($V_{SV} = V_{SH}$).

Two examples of VTI structures will be presented and only the case of a propagation along $\mathbf{e}_3$ is considered. We start by collecting some common results for this particular configuration (propagation along the vertical direction in a VTI structure) both using velocity averaging method and effective medium theory, Section 3.1. Next, two examples are given for specific VTI structure, Section 3.2. The first structure is quite artificial, with a c-axis having a unique $\theta = \theta_0$ value (and $\varphi \in [0, 2\pi]$), but it allows for explicit expressions of the velocities in both approaches. It could be seen as a girdle with vertical transverse isotropy, (*Azuma and Goto-Azuma*, 1996) with a single zenith angle, Fig. 3(a). The second example corresponds to a cone representative of clustered textures measured along ice cores (*Gusmeroli et al.*, 2012; *Diez and al.*, 2015), with $\theta \in [0, \theta_0]$ (and $\varphi \in [0, 2\pi]$) and it is studied numerically, Fig. 3(b).

3.1 The case of wave propagation along the vertical axis in a polycrystal with VTI

We collect here the simplifications which occur when we consider a wave propagating along the vertical axis, thus $\mathbf{k} = k(0, 0, 1)$, in a polycrystal with VTI, Fig. 3. The VTI structures have in common to allow for $\varphi \in [0, 2\pi]$, resulting in a distribution of c-axes given by probability distribution functions of the form

$$p(\theta, \varphi) = \frac{P_{\theta_0}(\theta)}{2\pi}, \quad \text{with} \int_0^{\pi/2} \mathrm{d}\theta \sin\theta \, P_{\theta_0}(\theta) = 1. \tag{15}$$

3.1.1 Velocities from the slowness averaging method

In this method, we first derive the velocities in a grain, and this is done for a wave propagating along $\mathbf{e}_3$. Thus, the Christoffel equation, Eq. (12) with $n_b = \delta_{b3}$ (same for n_c) simplifies to

$$\begin{vmatrix} \rho V^2 - C_{55} & -C_{45} & -C_{35} \\ -C_{45} & \rho V^2 - C_{44} & -C_{34} \\ -C_{35} & -C_{34} & \rho V^2 - C_{33} \end{vmatrix} = 0, \tag{16}$$

where C_{IJ} is derived from c_{ijkl} in Eq. (7), for a c-axis given by Eq. (6)

$$\begin{cases} C_{33} = As\theta^4 + 2(2L+F)s\theta^2 c\theta^2 + Cc\theta^4, \\ C_{44} = (A+C-2F)s\theta^2 c\theta^2 s\varphi^2 + L\left[s\varphi^2(c\theta^2 - s\theta^2)^2 + c\theta^2 c\varphi^2\right] + Ns\theta^2 c\varphi^2, \\ C_{55} = (A+C-2F)s\theta^2 c\theta^2 c\varphi^2 + L\left[c\varphi^2(c\theta^2 - s\theta^2)^2 + c\theta^2 s\varphi^2\right] + Ns\theta^2 s\varphi^2, \\ C_{34} = -s\varphi s\theta c\theta\left[As\theta^2 - Cc\theta^2 + (2L+F)(1-2s\theta^2)\right], \\ C_{35} = -c\varphi s\theta c\theta\left[As\theta^2 - Cc\theta^2 + (2L+F)(1-2s\theta^2)\right], \\ C_{45} = s\varphi c\varphi s\theta^2\left[(A+C-2F)c\theta^2 + L(1-4c\theta^2) - N\right], \end{cases} \tag{17}$$

and we have used the notations $c\varphi \equiv \cos\varphi$, $s\varphi \equiv \sin\varphi$, $s\theta \equiv \sin\theta$ and $c\theta \equiv \cos\theta$.

The discriminant, Eq. (22), can be calculated and we get the roots ρV^2

$$\begin{cases} \rho V^2 = \left(Lc\theta^2 + Ns\theta^2\right), \\ (\rho V^2)^2 + \left(As\theta^2 + Cc\theta^2 + L\right)\rho V^2 - F^2 s\theta^2 c\theta^2 + ACs\theta^2 c\theta^2 + ALs\theta^4 + CLc\theta^4 - 2FLs\theta^2 c\theta^2 = 0. \end{cases} \tag{18}$$

The first root correspond to a pure shear wave polarized in a direction perpendicular to both $\mathbf{k}$ and $\hat{\mathbf{c}}$, referred as SH-wave. The two roots of the second equation are associated to so-called quasi shear and quasi longitudinal waves, being coupled. The directions of polarization of the three waves are orthogonal (because the discriminant is associated to a symmetric matrix) but the quasi longitudinal wave is in general not along $\mathbf{e}_3$ and the quasi shear wave is in general not in the $(\mathbf{e}_1, \mathbf{e}_2)$ plane. More explicitly, the three velocities read

$$\begin{cases} \rho V_{SH}^2 = Lc\theta^2 + Ns\theta^2, \\ \rho V_{SV}^2 = \frac{1}{2}\left[C + L + (A-C)s\theta^2 - \sqrt{D}\right], \\ \rho V_P^2 = \frac{1}{2}\left[C + L + (A-C)s\theta^2 + \sqrt{D}\right], \end{cases} \tag{19}$$

$$\text{with} \quad D \equiv \left[As\theta^2 - Cc\theta^2\right]\left[As\theta^2 - Cc\theta^2 + 2L(c\theta^2 - s\theta^2)\right] + 4s\theta^2 c\theta^2(F^2 + 2FL) + L^2.$$

These are the expressions of the velocities in a single grain with a c-axis forming an angle θ with $\mathbf{e}_3$, Fig. 2. As expected from Section 2.2, the roots V^2 do not depend on φ, since the unique physical angle is θ formed by $\hat{\mathbf{c}}$ and $\mathbf{k}$ (φ is linked to the particular frame that is considered, and it will appear in the directions of the polarization of the elastic waves only).
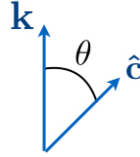
Figure 2. In a single crystal, the sound velocities depend only on θ.

The second step in the velocity averaging method can be applied

$$\frac{1}{V^{\mathrm{av}}(\theta_0)} = \int_0^{2\pi} \mathrm{d}\varphi \int_0^{\pi/2} \mathrm{d}\theta \, \sin\theta \, p(\theta,\varphi) V^{-1}(\theta,\varphi) = \int_0^{\pi/2} \mathrm{d}\theta \, \sin\theta \, P_{\theta_0}(\theta) V^{-1}(\theta), \qquad (20)$$

for $V = V_{SH}, V_{SV}, V_P$ taken from Eqs. (19). These last averages depend further on $P_{\theta_0}(\theta)$.

3.1.2 Velocities of the effective medium

With a probability function given by Eq. (15), the effective medium is characterized by a Voigt matrix

$$C_{IJ}^{\mathrm{eff}}(\theta_0) = \int_0^{2\pi} \frac{\mathrm{d}\varphi}{2\pi} \int_0^{\pi/2} \mathrm{d}\theta \, C_{IJ}(\theta,\varphi) \sin\theta \, P_{\theta_0}(\theta). \qquad (21)$$

The Voigt matrix $C_{IJ}(\theta,\varphi)$ has 21 coefficients, among which the 6 coefficients given in Eq. (17) (the other coefficients can be found in *Maurel et al.* (2015), Eqs. (3.6)-(3.7) in this reference). Averaging $C_{IJ}(\theta,\varphi)$ over $\varphi \in [0, 2\pi]$ makes 15 of them to vanish, and the resulting Voigt tensor has VTI symmetry, as expected, see Eqs. (A2)-(A3) in *Maurel et al.* (2015). The remaining integrations over θ depend on $P_{\theta_0}(\theta)$.

Next, the velocities of the elastic waves propagating along the axis $\mathbf{e}_3$ can be derived by solving the Christoffel equation, Eq. (12) with $c_{abcd} \to c_{ijkl}^{\mathrm{eff}}$. We get

$$\begin{vmatrix} \rho V^2 - C_{44}^{\mathrm{eff}}(\theta_0) & 0 & 0 \\ 0 & \rho V^2 - C_{44}^{\mathrm{eff}}(\theta_0) & 0 \\ 0 & 0 & \rho V^2 - C_{33}^{\mathrm{eff}}(\theta_0) \end{vmatrix} = 0, \qquad (22)$$

and we report below the intermediate result on C_{33} and C_{44} after φ-averaging

$$\begin{cases} \langle C_{33} \rangle_\varphi(\theta) = A\mathrm{s}\theta^4 + 2(2L+F)\mathrm{s}\theta^2\mathrm{c}\theta^2 + C\mathrm{c}\theta^4, \\ \langle C_{44} \rangle_\varphi(\theta) = L\mathrm{c}\theta^2 + N\mathrm{s}\theta^2, \end{cases} \qquad (23)$$

afterwards

$$C_{IJ}^{\mathrm{eff}}(\theta_0) = \int \mathrm{d}\theta \, \langle C_{IJ} \rangle_\varphi(\theta) \sin\theta \, P_{\theta_0}(\theta). \qquad (24)$$

The resulting effective velocities read

$$
\begin{cases}
V_P^{\mathrm{eff}} = \sqrt{C_{33}^{\mathrm{eff}}(\theta_0)/\rho}, \\
V_S^{\mathrm{eff}} = \sqrt{C_{44}^{\mathrm{eff}}(\theta_0)/\rho}.
\end{cases}
\tag{25}
$$

190 The longitudinal wave has a velocity associated to the vibration along $\mathbf{e}_3$; more importantly for the present demonstration, the two transverse waves have vibrations in the $(\mathbf{e}_1, \mathbf{e}_2)$ plane and *they are associated to the same velocity.*

3.2 Examples of the inconsistency in the slowness average method for polycrystals with VTI

3.2.1 Example 1: Girdle with vertical transverse isotropy and single θ_0 value

195 The first configuration is shown in Figure 3. It consists in a situation where all the grains within the polycrystal have the same angle $\theta = \theta_0$ but different φ randomly distributed in $[0, 2\pi]$. In this configuration, we have

$$
P_{\theta_0}(\theta) = \frac{\delta(\theta - \theta_0)}{\sin \theta_0}.
\tag{26}
$$

(a)   (b)
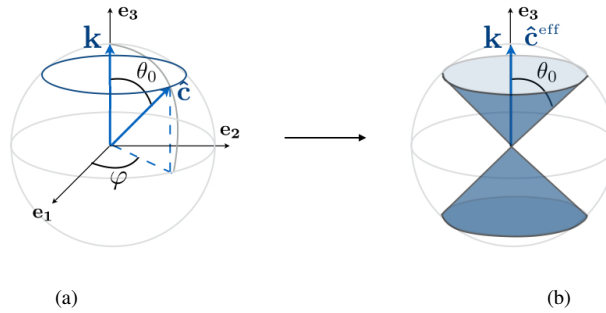
Figure 3. First configuration of thin girdle with Vertical Transverse Isotropy (a) typical c-axis $\hat{\mathbf{c}} = (\sin\theta_0 \cos\varphi, \sin\theta_0 \sin\varphi, \cos\theta_0)$ within one grain, θ_0 is fixed and φ varies randomly from grain to grain. (b) Resulting VTI texture of the polycrystal at the macroscopic scale. $\hat{\mathbf{c}}^{\mathrm{eff}}$ is the effective c-axis.

The velocities obtained from the slowness average method, Sec. 3.1.1, are obtained with V in Eqs.
200 (19) and Eqs. (20) and (26), leading to

$$
\begin{cases}
V_{SH}^{\mathrm{av}} = \sqrt{\dfrac{Lc\theta_0^2 + Ns\theta_0^2}{\rho}}, \\[2mm]
V_{SV}^{\mathrm{av}} = \sqrt{\dfrac{C + L + (A-C)s\theta_0^2 - \sqrt{D}}{2\rho}}, \\[2mm]
V_{P}^{\mathrm{av}} = \sqrt{\dfrac{C + L + (A-C)s\theta_0^2 + \sqrt{D}}{2\rho}},
\end{cases}
\tag{27}
$$

with $\quad D \equiv \left[As\theta_0^2 - Cc\theta_0^2 \right] \left[As\theta_0^2 - Cc\theta_0^2 + 2L(c\theta_0^2 - s\theta_0^2) \right] + 4s\theta_0^2 c\theta_0^2 (F^2 + 2FL) + L^2.$

These velocities are reported in Figs. 6 (red curves) and they will be commented latter.

We now derive the two shear and transverse velocities of the effective medium, Sec. 3.1.2, which are given by Eqs. (25) with $C_{IJ}^{\mathrm{eff}}(\theta_0) = \int \mathrm{d}\theta \, \langle C_{IJ}\rangle_\varphi(\theta)\sin\theta\, P_{\theta_0}(\theta)$, and Eqs. (23) and (26). We get

205
$$
\begin{cases}
V_P^{\mathrm{eff}} = \sqrt{\dfrac{1}{\rho}\left[A\mathrm{s}\theta_0^4 + 2(2L+F)\mathrm{s}\theta_0^2\mathrm{c}\theta_0^2 + C\mathrm{c}\theta_0^4\right]}, \\[2mm]
V_S^{\mathrm{eff}} = \sqrt{\dfrac{1}{2\rho}\left[(A+C-2F)\mathrm{s}\theta_0^2\mathrm{c}\theta_0^2 + L(4\mathrm{s}\theta_0^4 - 5\mathrm{s}\theta_0^2 + 2) + N\mathrm{s}\theta_0^2\right]},
\end{cases}
\tag{28}
$$

and these velocities are reported in black lines in Figs. 5 (they will be commented together with the results of the clustered texture with opening angle θ_0).

3.2.2 Example 2: the clustered texture with opening angle θ_0

This texture is shown in Fig. 4. It corresponds to

210
$$
P_{\theta_0}(\theta) = \frac{H_{\theta_0}(\theta)}{1 - \cos\theta_0},
\tag{29}
$$

where H_{θ_0} is the rectangular function, equals unity for $0 \leq \theta \leq \theta_0$, zero otherwise.

(a)   (b)
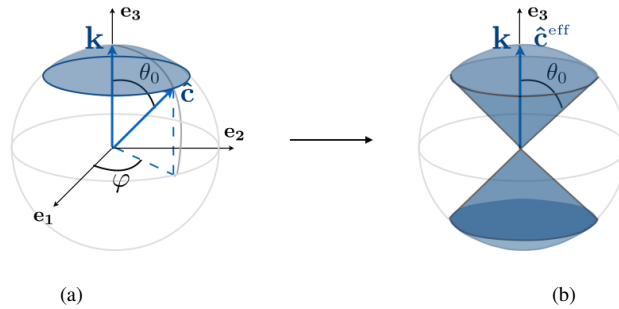
Figure 4. Second configuration, the usual clustered texture, with Vertical Transverse Isotropy (a) typical c-axis $\hat{\mathbf{c}} = (\sin\theta\cos\varphi, \sin\theta\sin\varphi, \cos\theta)$ within one grain, θ varies in $[0,\theta_0]$ and φ varies randomly from grain to grain. (b) Resulting clustered, VTI, texture of the polycrystal at the macroscopic scale. $\hat{\mathbf{c}}^{\mathrm{eff}}$ is the effective c-axis.

The velocities $(V_{SH}^{\mathrm{av}}, V_{SV}^{\mathrm{av}}, V_P^{\mathrm{av}})$ in the slowness average method, Sec. 3.1.1, cannot be calculated analytically in this case. The average on θ in Eq. (20) is performed numerically (with Eqs. (19) and (29)).

215   The velocities of the effective medium ($V_S^{\text{eff}}, V_P^{\text{eff}}$, Sec. 3.1.2) are calculated as previously, using Eqs. (23) to (25), with Eq. (29), and we get

$$
\text{Cluster}
\begin{cases}
V_S^{\text{eff}} = \sqrt{\dfrac{(L+N)}{2\rho} + \dfrac{[2(A+C)-4F-3L-5N]}{30\rho}X - \dfrac{[(A+C)-2(2L+F)]}{10\rho}Y} \\[2ex]
V_P^{\text{eff}} = \sqrt{\dfrac{A}{\rho} + \dfrac{[-7A+3C+4(2L+F)]}{15\rho}X + \dfrac{[A+C-2(2L+F)]}{5\rho}Y}
\end{cases}
\tag{30}
$$

with $X \equiv 1 + \cos\theta_0 + \cos^2\theta_0$ and $Y \equiv \cos^3\theta_0 + \cos^4\theta_0$. These values are reported in black lines in Fig. 6.
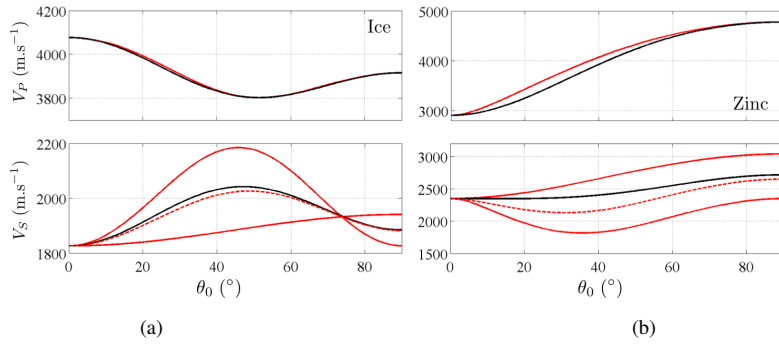
Figure 5. Illustration of the inconsistency of the slowness average method for the girdle texture with single zenith value θ_0, for ice (a) and for zinc (b). The wave propagation is along $\mathbf{e}_3 = \hat{\mathbf{c}}$ (Fig. 4) for which $V_S = V_{SH} = V_{SV}$. Black curves show the velocities V_P^{eff} and V_S^{eff} of the effective medium as a function of θ_0, Eqs. (30); Red lines show the velocity V_P^{av} and the two -unphysical- velocities of the S-waves $V_{SH}^{\text{av}}, V_{SV}^{\text{av}}$; dashed red line indicates the S-velocity resulting from the average of the S-slowness, as used in *Middya et al.* (1986).
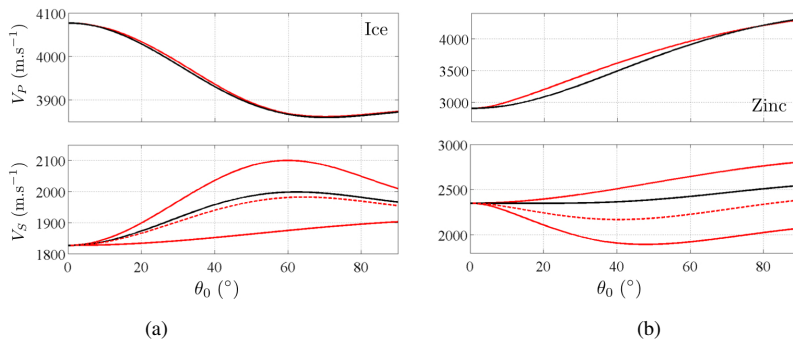
Figure 6. Same representation as in Fig. 5 for VTI structure with a cone of aperture angle θ_0.

Let us now comment the Figs. 5 and 6. In both cases, the velocities of shear and longitudinal waves have been reported for physical properties of ice and zinc assuming a girdle texture with single zenith angle θ_0 (Fig. 3) and a clustered texture with aperture angle θ_0 (Fig. 5), respectively. Black lines correspond to the velocities V_P^{eff} and V_S^{eff} and as previously said, a unique velocity V_S^{eff} is found from the effective medium theory, by construction (we say here by construction because the effective medium ensures the expected anisotropy at large scale since the effective elastic tensor is averaged). This is consistent with the considered VTI symmetry and the observed variations of the velocities with θ_0 are typically the kind of data that will be used in the inverse problem to get information about the variation of the texture with depth in borehole sonic logging (*Maurel et al.*, 2015). We use these velocities as reference velocities in the following.

The plain red lines refer to the velocities V_P^{av} and $(V_{SH}^{\text{av}}, V_{SV}^{\text{av}})$ extracted from the slowness average method. We have already commented that the two shear velocities obtained are unphysical since a unique shear velocity is expected. The discrepancy observed is significant for the shear velocities (with respect to the reference value, in black) both in the case of ice and zinc in Figs. 5 and 6. For the longitudinal velocity, the discrepancy is incidental in the case of ice but may become more significant, as illustrated here for zinc. This is why the case of zinc has been reported (zinc single crystals being more elastically anisotropic than ice single crystals, the discrepancies are more noticeable).

The two different shear velocities should have been observed in *Diez and Eisen* (2015) where the average velocity method is used for cone textures, using numerical averages (note an ambiguity in the definitions of the averages in the Eqs. (12) and (13) in this reference, where the $\sin\theta$ seems to be missing for averaging over the spherical angles). Possibly, the authors use an additional average for the shear velocity, as suggested by *Middya et al.* (1986), namely $V_S = 1/2(V_{SV} + V_{SH})$. This latter average is unjustified and it is not expected that it has to be close to the reference value (black curves). In Figs. 5 and 6, these velocities V_S are reported in dotted red lines. Although these lines are quite close from the reference one for ice, they remain significantly far away for zinc. Besides, it is not guaranteed that higher errors would not be obtained for other textures.

4 Comment on Bennett's derivation of the velocities in the usual clustered texture

In this section, we analyze the derivation proposed by Bennett to get the velocities in clustered polycrystal (*Bennett*, 1968). Basically, the error in Bennet's calculation lies in the expression of the sound speed in single crystal, that is at the scale of the grain. Then, the average is correctly conduced but starting from unphysical velocities. Remember that the velocities in a single crystal is given by Eqs. (19), and they depend only on the angle θ between the wavenumber $\mathbf{k}$ and the direction $\hat{\mathbf{c}}$ of the c-axis.

4.1 Reporting Bennet's calculations

To be clear, the error in Bennett's calculation appears in the fact that he obtains at some point the

255 following expressions of the sound velocities for wave propagation in single ice

> **Bennett's unphysical expressions for the sound velocities in single crystal**
> $$\begin{cases} \dfrac{1}{V_{SH}} = S_{SH} = (a_2 + b_2) - 8b_2 \sin^2 \varphi \cos^2 \theta \sin^2 \theta - 2b_3 \cos^2 \varphi \sin^2 \theta, \\[2mm] \dfrac{1}{V_{SV}} = S_{SV} = (a_2 + b_2) - 8b_2 \cos^2 \varphi \cos^2 \theta \sin^2 \theta - 2b_3 \sin^2 \varphi \sin^2 \theta. \end{cases}$$ (31)

see Eqs. (5-15) in *Bennett* (1968), and here we have adapted his notations to ours. These expressions are found in the case where the wave propagates along $\mathbf{e}_3$ with a c-axis along the direction $\hat{\mathbf{c}} = (\sin \theta \cos \varphi, \sin \theta \sin \varphi, \cos \theta)$, see Fig. 7(b). These expressions do not agree with Eqs. (19) and

260 beside, the dependance of V_{SV} and V_{SH} on φ is unphysical, as previously said: it is clear that the angle θ is the unique angle that is needed, and in fact, the unique angle that can be defined, see Fig. 2. Bennett did not publish his calculations. They can be found in his thesis but for the sake of completeness, we report below the main steps of these calculations (also the correspondances with Bennett's notations are given).

265   Bennett starts with the slownesses in a single crystal, called $S = 1/V$ and which are given by

$$\begin{cases} S_1 = S_P \simeq a_1 - b_1 \cos 4\theta - c_1 \cos 2\theta, \\ S_2 = S_{SV} \simeq a_2 + b_2 \cos 4\theta, \\ S_3 = S_{SH} \simeq a_3 + b_3 \cos 2\theta. \end{cases}$$ (32)

The above expressions are correct, although approximate and they are close to the Thomsen approximations (*Thomsen*, 1986), see also a discussion in *Maurel et al.* (2015). They correspond to approximated forms of the inverses of the velocities in single crystals given in Eqs. (19).

270   In the above expressions, θ (the usual azimuthal angle in spherical coordinates) is the angle $(\mathbf{k}, \hat{\mathbf{c}})$ because of the chosen frame, see Fig. 7(b). Bennett decided to use a different frame where neither $\mathbf{k}$ nor $\hat{c}$ are along $\mathbf{e}_3$, and he denoted $\hat{\theta} \equiv (\mathbf{k}, \hat{\mathbf{c}})$. The story should end there: it is sufficient to replace θ by $\hat{\theta}$ in Eqs. (32) to get the slowness expressions. This is not what Bennett did, and this is the source of the error in his result.

275   The new multiple angles in Fig. 7(a) are defined as follows $\sigma \equiv (\mathbf{k}, \mathbf{e}_3)$, $\hat{\theta} \equiv (\mathbf{k}, \hat{\mathbf{c}})$ and $\theta = (\hat{\mathbf{c}}, \mathbf{e}_3)$; also, the angle $\hat{\varphi}$ is defined as the angle between the planes $(\mathbf{k}, \mathbf{e}_3)$ and $(\mathbf{k}, \hat{\mathbf{c}})$ (this angle is not represented in Fig. 7(a), it will be equivalent and more consistent to define it between the two vectors normal to these planes).

    It is straightforward to remark that for $\sigma = 0$, we recover $\theta = \hat{\theta}$ and it is essential that Eqs. (32)

280 are recovered in this case.
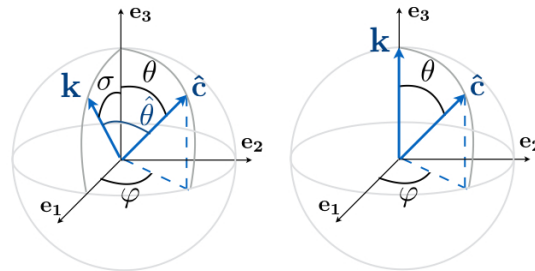
Figure 7. (a) System of angles used in Bennett's calculations. $\hat{c}$ is given by (φ, θ) and $\mathbf{k}$ is given by σ, being otherwise in the $(\mathbf{e}_1, \mathbf{e}_3)$ plane. The extra angle $\hat{\theta}$ denotes the angle between $\mathbf{k}$ and $\hat{c}$, thus $\cos\hat{\theta} = \sin\sigma\cos\varphi\sin\theta + \cos\sigma\cos\theta$. (b) Particular case of the Bennett configuration, for $\sigma = 0$; in this case, $\hat{\theta} = \theta$.

An ensemble of relations between the different angles are then derived by Bennett, among which $\cos\hat{\theta} = \sin\sigma\cos\varphi\sin\theta + \cos\sigma\cos\theta$ and

$$
\begin{cases}
\sin^2\hat{\varphi} = \dfrac{\sin^2\varphi\sin^2\theta}{\sin^2\hat{\theta}}, \\[2mm]
\cos^2\hat{\varphi} = \dfrac{(\cos\sigma\cos\varphi\sin\theta - \sin\sigma\cos\theta)^2}{\sin^2\hat{\theta}}
\end{cases}
\tag{33}
$$

and these relations are correct, notably, at this stage, if $\sigma = 0$, then $\hat{\theta} = \theta$ and $\hat{\varphi} = \varphi$.

285   The next step is the source of the error. It is said that the slowness of the wave depends on $\hat{\varphi}$ following

$$
\begin{cases}
S_P = S_1, \\
S_{SV} = S_2\cos^2\hat{\varphi} + S_3\sin^2\hat{\varphi}, \\
S_{SH} = S_2\sin^2\hat{\varphi} + S_3\cos^2\hat{\varphi}.
\end{cases}
\tag{34}
$$

This is announced by Bennett as an intuitive approximation. Obviously (see Eqs. (33)), $\hat{\varphi}$ can vary while $\hat{\theta}$ remains constant, from which the above equations pretend that the velocity of the shear

290   waves depend on something else than on $\hat{\theta}$ only, and this is incorrect, from Eq. (32). More explicitly, using $\sigma = 0$ (thus, $\hat{\theta} = \theta$, $\hat{\varphi} = \varphi$) in the Eq. (34) and using Eqs. (32)-(33), we get the Eqs. (31) which contain clearly a mistake.

Starting from these false expressions of the shear velocities for single crystals, Bennett derived the averaged slownesses by means of an average equivalent to an average over φ and θ in Eqs. (31).

295   In fact by construction of the weighted forms in the Eq. (34) (and the same for Eq. (31)), the same value for the two averaged slownesses S_{SH} and S_{SV} is obtained. Unfortunately, these expressions are not reliable.

5 Conclusions

In this paper, we have proposed a critical analysis of the velocity, or slowness, average methods as
300 recently used in the post treatment of the velocities deduced from borehole sonic logging measure-
ments. Although this method is justified in particular cases, as the wave propagation in stratified
media (and it is used for seismic waves in this quasi one-dimensional context), it presents signif-
icant pitfalls in the context of the propagation in ice polycrystals. Basically, the slowness average
method is based on the qualitative argument that the times of flight of the waves in each grains can
305 be added, and this vision is based on the ray theory. Ray theory means high frequency, namely the
wave propagates, between two interfaces, over large distances compared to its wavelength (*Kohnen*,
1974; *Blankenship et al.*, 1987). This is not the case in sonic logging measurements, with elastic
wavelengths of the order of a few tens of centimeters while the typical grain sizes range from a
few millimeters to tens of centimeters. Qualitatively, good trends in the variations of the velocities
310 are obtained and possibly it is sufficient for crude predictions, as the presence of liquid in rocks
or the detection of rock cracks. In the case of a prediction in a change of ice texture with depths,
the variations in the elastic velocities are weak and care has to be taken not to introduce additional
uncertainties because of a too crude approximation in the theoretical model. This is why a reliable
approach, based on the calculation of an effective medium, has to be retained. Such approach prop-
315 erly describes the modifications in the elastic velocities associated with ice texture (*Maurel et al.*,
2015), and it can be used for further inversion of sonic logger data extracted along ice cores.

References

Azuma, N., and Goto-Azuma, K. (1996). An anisotropic flow law for ice-sheet ice and its implications. Annals of Glaciology, 23, 202-208.

320 Bennett H.F. 1968 An investigation into velocity anisotropy through measurements of ultrasonic wave velocities in snow and ice cores from Green- land and Antarctica. Ph.D. thesis, University of Wisconsin, Madison, 1968.

Blankenship, D. D., Bentley, C. R., Rooney, S. T., and Alley, R. B. (1987). Till beneath Ice Stream B: 1. Properties derived from seismic travel times. Journal of Geophysical Research: Solid Earth (1978 - 2012), 325 92(B9), 8903-8911.

Diez, A., and Eisen, O. (2015). Seismic wave propagation in anisotropic ice-Part 1: Elasticity tensor and derived quantities from ice-core properties. The Cryosphere, 9(1), 367-384.

Diez, A., Eisen, O., Hofstede, C., Lambrecht, A., Mayer, C., Miller, H., Weikusat, I. (2015). Seismic wave propagation in anisotropic ice-Part 2: Effects of crystal anisotropy in geophysical data. The Cryosphere, 330 9(1), 385-398.

Diez, A., and Eisen, O. (2015). Seismic wave propagation in anisotropic ice-Part 1: Elasticity tensor and derived quantities from ice-core properties. The Cryosphere, 9(1), 367-384.

Gusmeroli, A., Pettit, E. C., Kennedy, J. H., and Ritz, C. (2012). The crystal fabric of ice from full?waveform borehole sonic logging. Journal of Geophysical Research: Earth Surface (2003-2012), 117(F3).

335 Keller JB. 1964 Stochastic Equations and Wave Propagation in Random Media. in *Proceedings of the 16th Symposium on Applied Mathematics* (AMS, New York, 1964) 145-179.

Karal Jr FC, Keller JB. 1964 Elastic, Electromagnetic and Other Waves in Random medium. *J. Math. Phys.* **5** 537-547.

340 Kohnen, H. (1974). The temperature dependence of seismic waves in ice. J. Glaciol, 13(67), 144-147.

Maurel, A., Lund, F., and Montagnat, M. (2015, May). Propagation of elastic waves through textured polycrystals: application to ice. In Proceedings of the Royal Society of London A: Mathematical, Physical and Engineering Sciences (Vol. 471, No. 2177, p. 20140988). The Royal Society.

Middya, T. R., Paul, M., and Basu, A. N. (1986). Multiple scattering theoretical and computer simulated dy-345 namic model approaches to effective elastic properties of randomly disordered composites. Journal of applied physics, 59(7), 2376-2381.

Thomsen GW. 1986 Weak elastic anisotropy. *Geophysics* **15** 1954-1966.

Thorsteinsson T. 1990 Textures and fabrics in bottom silty ice from the Dye 3 ice core. University of Copenhagen, MS thesis.

350 Voigt W. 1928 Lehrbuch der Kristallphysik, reprint of the 1st edn. Leipzig: Teubner.

Vélez, J. A., Tsoflias, G. P., Black, R. A., Van der Veen, C. J. and Anandakrishnan, S. (2016). Distribution of preferred ice crystal orientation determined from seismic anisotropy: Evidence from Jakobshavn Isbræand the North Greenland Eemian Ice Drilling facility, Greenland. Geophysics, 81(1), WA111-WA118.